Research Article | Vol. 26, No. 7 | 2 Apr 2018 | OPTICS EXPRESS 8364
Optics EXPRESS

Polarization-sensitive pulse reconstruction by momentum-resolved photoelectron streaking

KAY WALTAR,[1,*] JOHANNES HAASE,[2] MATTEO LUCCHINI,[3] JEROEN A. VAN BOKHOVEN,[2,4] MATTHIAS HENGSBERGER,[1] JÜRG OSTERWALDER,[1] AND LUCA CASTIGLIONI[1]

[1]*Department of Physics, University of Zürich, 8057 Zürich, Switzerland*
[2]*Laboratory for Catalysis and Sustainable Chemistry, Paul Scherrer Institute, 5232 Villigen-PSI, Switzerland*
[3]*Physics Department, Politecnico di Milano, 21033 Milan, Italy*
[4]*Department of Chemistry, ETH Zurich, 8093 Zürich, Switzerland*
[*]*waltar@physik.uzh.ch*

Abstract: The precise knowledge of the electric field in close proximity to metallic and dielectric surfaces is a prerequisite for pump-probe experiments aiming at the control of dynamic surface processes. We describe a model to reconstruct this electric field in immediate surface proximity from data taken in photoelectron THz-streaking experiments with an angle-resolved electron analyzer. Using Monte-Carlo simulations we are able to simulate streaking experiments on arbitrary surfaces with a variety of initial electron momentum distributions and to reconstruct the effective electric field at the surface. Our results validate the approach and suggest energy regimes for optimal pulse reconstruction.

OCIS codes: (320.0320) Ultrafast optics; (320.7100) Ultrafast measurements.

References and links

1. S. S. Dhillon, M. S. Vitiello, E. H. Linfield, A. G. Davies, M. C. Hoffmann, J. Booske, C. Paoloni, M. Gensch, P. Weightman, G. P. Williams, E. Castro-Camus, D. R. S. Cumming, F. Simoens, I. Escorcia-Carranza, J. Grant, S. Lucyszyn, M. Kuwata-Gonokami, K. Konishi, M. Koch, C. A. Schmuttenmaer, T. L. Cocker, R. Huber, A. G. Markelz, Z. D. Taylor, V. P. Wallace, J. A. Zeitler, J. Sibik, T. M. Korter, B. Ellison, S. Rea, P. Goldsmith, K. B. Cooper, R. Appleby, D. Pardo, P. G. Huggard, V. Krozer, H. Shams, M. Fice, C. Renaud, A. Seeds, A. Stöhr, M. Naftaly, N. Ridler, R. Clarke, J. E. Cunningham, and M. B. Johnston, "The 2017 terahertz science and technology roadmap," J. Phys. D Appl. Phys. **50**(4), 043001 (2017).
2. J. L. LaRue, T. Katayama, A. Lindenberg, A. S. Fisher, H. Öström, A. Nilsson, and H. Ogasawara, "THz-Pulse-Induced Selective Catalytic CO Oxidation on Ru," Phys. Rev. Lett. **115**(3), 036103 (2015).
3. M. Greif, T. Nagy, M. Soloviov, L. Castiglioni, M. Hengsberger, M. Meuwly, and J. Osterwalder, "Following the molecular motion of near-resonant excited CO on Pt(111): a simulated x-ray photoelectron diffraction study based on molecular dynamics," Struct. Dyn. **2**(3), 035102 (2015).
4. M. Garg, M. Zhan, T. T. Luu, H. Lakhotia, T. Klostermann, A. Guggenmos, and E. Goulielmakis, "Multi-petahertz electronic metrology," Nature **538**(7625), 359–363 (2016).
5. R. Kienberger, E. Goulielmakis, M. Uiberacker, A. Baltuska, V. Yakovlev, F. Bammer, A. Scrinzi, T. Westerwalbesloh, U. Kleineberg, U. Heinzmann, M. Drescher, and F. Krausz, "Atomic transient recorder," Nature **427**(6977), 817–821 (2004).
6. I. Walmsley and V. Wong, "Characterisation of the electric field of ultrashort optical pulses," J. Opt. Soc. Am. B **13**(11), 2453–2463 (1996).
7. C. Dorrer and I. Kang, "Complete temporal characterization of short optical pulses by simplified chronocyclic tomography," Opt. Lett. **28**(16), 1481–1483 (2003).
8. D. Kane and R. Trebino, "Characterisation of Arbitrary Femtosecond Pulses Using Frequency-Resolved Optical Gating," IEEE J. Quantum Electron. **29**(2), 571–579 (1993).
9. F. Quére, Y. Mairesse, and J. Itatani, "Temporal characterisation of attosecond XUV fields," J. Mod. Opt. **52**(2-3), 339–360 (2005).
10. Q. Wu and X.-C. Zhang, "Free-space electro-optic sampling of terahertz beams," Appl. Phys. Lett. **67**(24), 3523–3525 (1995).
11. S.-G. Park, M. R. Melloch, and A. M. Weiner, "Comparison of terahertz waveforms measured by electro-optic and photoconductive sampling," Appl. Phys. Lett. **73**(22), 3184–3186 (1998).
12. J. Itatani, F. Quéré, G. L. Yudin, M. Yu. Ivanov, F. Krausz, and P. B. Corkum, "Attosecond Streak Camera," Phys. Rev. Lett. **88**(17), 173903 (2002).

#321045 https://doi.org/10.1364/OE.26.008364
Journal © 2018 Received 31 Jan 2018; revised 13 Mar 2018; accepted 16 Mar 2018; published 22 Mar 2018

Optics EXPRESS

13. F. O. Kirchner, A. Gliserin, F. Krausz, and P. Baum, "Laser streaking of free electrons at 25 keV," Nat. Photonics **8**(1), 52–57 (2014).
14. F. Krausz and M. Ivanov, "Attosecond physics," Rev. Mod. Phys. **81**(1), 163–234 (2009).
15. Y. Mairesse and F. Quere, "Frequency-resolved optical gating for complete reconstruction of attosecond bursts," Phys. Rev. A **71**(1), 011401 (2005).
16. M. Kitzler, N. Milosevic, A. Scrinzi, F. Krausz, and T. Brabec, "Quantum Theory of Attosecond XUV Pulse Measurement by Laser Dressed Photoionization," Phys. Rev. Lett. **88**(17), 173904 (2002).
17. L. Castiglioni, D. Leuenberger, M. Greif, and M. Hengsberger, "Attosecond Transversal Streaking to Probe Electron Dynamics at Surfaces," in Multiphoton Processes and Attosecond Physics, K. Yamanouchi, and M. Katsumi, eds. (Springer, 2012), pp. 365–368.
18. M. Lucchini, A. Ludwig, L. Kasmi, L. Gallmann, and U. Keller, "Semi-classical approach to compute RABBITT traces in multi-dimensional complex field distributions," Opt. Express **23**(7), 8867–8879 (2015).
19. H. G. Muller, "Reconstruction of attosecond harmonic beating by interference of two-photon transitions," Appl. Phys. B **74**(S1), S17–S21 (2002).
20. M. Lucchini, L. Castiglioni, L. Kasmi, P. Kliuiev, A. Ludwig, M. Greif, J. Osterwalder, M. Hengsberger, L. Gallmann, and U. Keller, "Light-Matter Interaction at Surfaces in the Spatiotemporal Limit of Macroscopic Models," Phys. Rev. Lett. **115**(13), 137401 (2015).

1. Introduction

The availability of intense THz laser pulses in recent years enables new types of pump-probe experiments. Intense THz fields can be used to drive and control dynamic processes in solids and at solid surfaces [1]. In particular, THz-induced surface catalytic reactions have recently gained much scientific interest [2]. A THz electric field can stimulate atomic motion in adsorbed molecules by interaction with their dipole moment [3]. Depending on the polarization of the exciting field, this can selectively facilitate catalytic reactions, such as molecular dissociation or oxidation of carbon monoxide, for instance. The time-dependent distribution and polarization of the electric field in immediate surface proximity are thus decisive experimental parameters. A pulse metrology that enables the reconstruction of both field polarization and shape is thus a prerequisite to any quantitative study of THz-induced surface catalytic reactions.

Versatile temporal characterization procedures for short light pulses have been available for a few decades [4–7]. Among the most frequently employed are the concepts of frequency-resolved optical gating (FROG) [8], spectral phase interferometry for direct electric-field reconstruction (SPIDER) [9], electro-optic sampling (EOS) [10,11] and the streaking experiments [12,13]. Most concepts have been modified to reconstruct electric field pulses of attosecond duration in the extreme-ultraviolet (XUV) regime [14–17]. While FROG and SPIDER directly characterize the initial laser pulse by all-optical means, the streaking experiment uses photoelectrons as intermediates. An applied laser field changes the electron momentum distribution, which can then be detected with a suitable electron analyzer after interaction. The analyzer must be capable of simultaneously detecting both the electron kinetic energy and direction of motion, like e.g. an angle-resolved time-of-flight spectrometer or a 2D hemispherical analyzer. From the modified momentum distributions, conclusions on the nature of the interacting laser field can be drawn.

In the case of experiments on solid surfaces, this effective interacting field is often the result of a superposition of the incoming and reflected laser pulse in close proximity of the surface. So far, the reconstruction of this effective electric field from laser-field-modified electron momentum distributions has not been directly pursued. We discuss a simple model to reconstruct the near-field polarization and effective amplitude of THz pulses incident on metallic and dielectric surfaces and interfaces by means of photoelectron streaking of non-relativistic electrons [17]. Lucchini et al. have developed a semi-classical Monte-Carlo model of electron momentum changes in complex 2D field gratings [18] in order to calculate RABBITT (Reconstruction of Attosecond Beating By Interference of Two-photon Transitions) traces [19]. This model was used later to validate the Fresnel equations in attosecond pump-probe experiments [20]. We extend this model to simulate photoelectron pump-probe experiments of XUV-photoemitted electrons interacting with THz-pulses of

Optics EXPRESS

several picoseconds duration and arbitrary polarization. These simulations provide the electron momentum distributions as a function of pump-probe delay from which we reconstruct the effective electric field distribution at a variety of distinct interfaces, described by their optical constants. The combination of short XUV pulses with few-cycle THz pulses has recently become widely available at free-electron laser (FEL) facilities as well as using tabletop high-harmonic generation (HHG) sources.

2. Method

We assume a pump-probe set-up in which photoelectrons are initially generated by a short XUV pulse in a solid sample. Subsequently, these electrons undergo a momentum change due to the interaction with a few-cycle THz pulse. With an electron analyzer capable of detecting both the kinetic energy and the angular distribution of the emitted electrons simultaneously, momentum changes of the electrons can be tracked. For a linearly polarized field the components parallel ($E_{\parallel}$) and perpendicular ($E_{\perp}$) to the sample surface lead to distinct modifications in the photoelectron momentum distribution (Figs. 1(a) and 1(b), respectively). An experimental prerequisite for the simultaneous detection of both contributions, $E_{\parallel}$ and $E_{\perp}$, is the orientation of the angular dispersive axis of the electron analyzer along the direction parallel to the surface, along which the electric field component $E_{\parallel}$ is to be reconstructed. In each angular channel of the electron analyzer the energetic center of mass (COM), for example the position of an elastic photoemission line, can be experimentally determined and the shift of the COM position due to photoelectron streaking serves as measure for the streaking field. COM positions as a function of detection angle are represented by the solid and dotted lines in Fig. 1(c): The distinct influences of differently polarized field components on the photoelectron momentum distribution are shown. A component polarized parallel to the surface leads to a lateral shift of the momentum distribution, and thereby to an energy shift, which is roughly anti-symmetric with respect to the normal direction. This is visible as a linear tilt in the energy COM with respect to the angle-dispersive axis. A perpendicularly polarized component causes a symmetric change in momentum for positive and negative angular channels and an energy-offset with respect to the interaction-free distribution. Using these two distinct influences, the streaking field at the sample surface can be reconstructed.

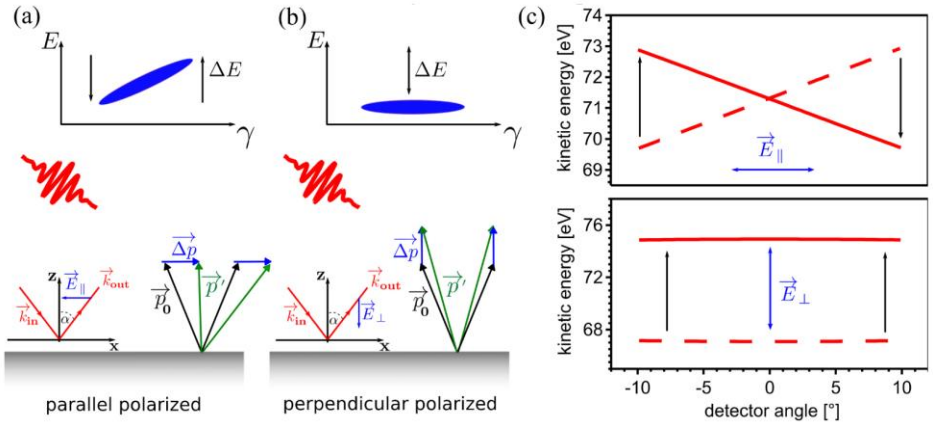

Fig. 1. (a, b) Schematic illustration of the distinct influences of field components parallel and perpendicular to the surface ($E_{\parallel,\perp}$) on the momentum change of XUV-emitted photoelectrons. Here, $\mathbf{p}_0$ represents the initial momentum, $\Delta\mathbf{p}$ the field induced momentum change and $\mathbf{p}'$ the final electron momentum. The angle of light incidence is denoted by α. The wavevectors of the incoming and reflected THz-pulse are represented by $\mathbf{k}_{in}$ and $\mathbf{k}_{out}$. γ is the angle of electron detection, i.e. the detector angle. (c) Detector images with energetic and angular resolution for field extrema with opposite sign. During interaction with the electric field, the COM projection of the electrons will oscillate between the two extrema represented by the dashed and solid lines.

Optics EXPRESS

The amplitude and temporal shape of both electric field polarizations can be obtained from two features of the detected final electron momentum distribution. A kinetic energy offset, defined as the difference in electron COM energy with and without the laser field interaction along normal emission, is a measure of the perpendicular component. The tilt angle of the slopes in Fig. 1(c) depends on the electric field component parallel to the surface ($E_{\parallel}$). The perpendicular field-component ($E_{\perp}$) causes no angular modification at normal emission, i.e. the electrons do not leave their initial angular channel. The total momentum gain thus appears as a change in the electron kinetic energy. It is possible to derive an analytical solution for the modulus of the momentum change as a function of the kinetic energy offset (see appendix for derivation).

$$|\Delta\mathbf{p}| = |\mathbf{p}|\left(\sqrt{1+\frac{2m\Delta E}{|\mathbf{p}|^2}}-1\right) = \sqrt{2mE}\left(\sqrt{1+\frac{\Delta E}{E}}-1\right) \tag{1}$$

Here, E is the initial kinetic energy of the electron, ΔE is the energy shift due to the interaction with the THz-field and $\mathbf{p}$ is the initial momentum. For the parallel field component, the THz interaction leads to both an energy and angular modification. Measuring the energy COM in an arbitrary angular channel does not provide information on the initial momentum direction of the electron. Therefore, information on the absolute angular modification is missing and no unambiguous solution to the absolute momentum change can be derived. However, the orientation of the momentum change relative to the angular dispersive axis of the analyzer is an indication of the momentary tilt direction. The magnitude of the momentum change can be obtained by a fitting procedure. A suitable model, comprising the electron momentum change in absolute value and direction as a function of input electric field strength has to be fitted to the experimentally determined tilt angle at every instant in time. The total momentum change for both field components is then related to a total acting vector potential by

$$\Delta p_{\parallel/\perp} = e\int_{\tau}^{\infty}\left[\mathbf{E}_{\text{in}}(t,\mathbf{r})+\mathbf{E}_{\text{out}}(t,\mathbf{r})\right]\cdot\mathbf{n}_{\parallel,\perp}\,\mathrm{d}t = -e\mathbf{A}(\tau,\mathbf{r})\cdot\mathbf{n}_{\parallel,\perp}. \tag{2}$$

Here $\mathbf{E}_{\text{in}}$ and $\mathbf{E}_{\text{out}}$ are the electric field components of the incoming and outgoing THz fields in the vicinity of the surface and $\mathbf{n}_{\parallel,\perp}$ are the unit vectors either parallel or perpendicular to the surface. τ is the instant of photoexcitation by the probing XUV pulse. The last equality in Eq. (2) holds when the electron motion can be neglected during the THz interaction since the position vector $\mathbf{r}$ is generally a function of time. In all numerical simulations performed herein, the electron motion is incorporated. The amplitude of the electric field is obtained by taking the derivative of the vector potential as a function of time following Maxwell's equations. In this way, the effective electric field components can be determined using

$$\mathrm{E}_{\parallel,\perp}(t,\mathbf{r}) = -\frac{\mathrm{d}\mathrm{A}_{\parallel,\perp}(t,\mathbf{r})}{\mathrm{d}t}. \tag{3}$$

Figure 2 shows the simulated change in electron kinetic energy due to interaction with a THz pulse. A Gaussian-shaped electric field distribution with a peak amplitude of 10^7 V/m is used for polarizations parallel and perpendicular to the surface. These results are obtained by calculating the vector potential from the known initial electric field. The direction and magnitude of the vector potential at the time of electron emission determine the total momentum change following Eq. (2). A vector addition then yields the final electron momentum. In Figs. 2(b) and 2(c) the final kinetic COM energy is displayed color-coded as function of detection angle at different times of photoexcitation. A vertical cut along these graphs results in the COM distributions that are shown in Fig. 1(c). The apparent phase shift between positive and negative angular channels in Fig. 2(b) is a consequence of the tilted energy distribution with respect to the final detection direction, and is a clear hallmark of

Optics EXPRESS

electric field components polarized parallel to the surface. A perpendicularly polarized field leads to a symmetric kinetic energy offset (Fig. 2(c)).

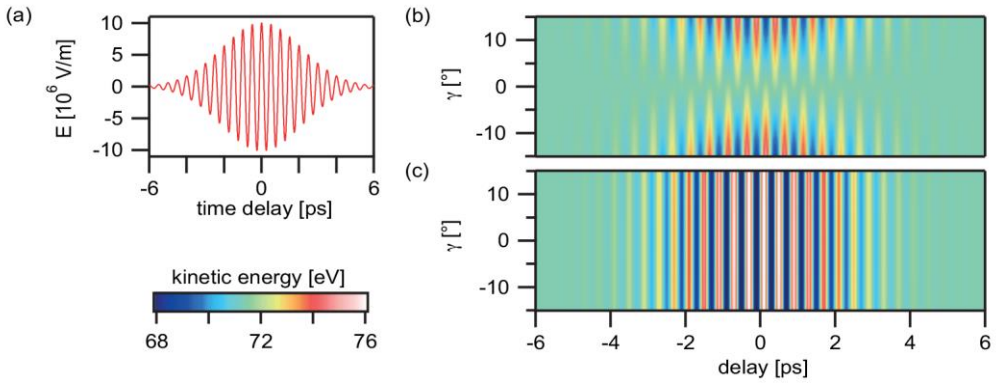

Fig. 2. (a) Temporal shape of the incident Gaussian THz pulse (λ = 150 µm, FWHM = 5 ps) with an amplitude of 10^7 V/m. (b, c) Photoelectron COM energy as a function of detection angle at different times of photoexcitation for a THz field polarization parallel (b) and perpendicular (c) to the surface. The initial kinetic energy of the photoelectrons is 72 eV.

In order to validate our model, we analyze pump-probe photoelectron-momentum maps generated by a semi-classical Monte-Carlo simulation using our method. We assume that electrons on their path to the analyzer undergo a momentum change while travelling through a transient grating. This 2D field grating is present at the sample surface due to a superposition of the incoming and reflected THz pulses. The initial emission angle, kinetic energy and time of photoexcitation of the electrons are chosen as random variables. They determine the initial conditions for the differential equation of motion of the photoelectrons. The effective, instantaneous electric field calculated using Fresnel's equations at each instant exerts the sole external force on the electrons outside the sample surface. Eventually, the final momentum distribution is convolved with a rectangular transmission function representing the limited range of detector transmission in a real experiment.

3. Results

We will discuss the applicability of our model by reconstructing the effective near-surface THz-field for a set of experimental parameters. The angle of incidence of the incoming THz-pulse and the Gaussian temporal shape are kept constant in all simulations. In addition, the parameter space is confined by choosing three distinct substrates, namely a completely transparent (n = 1, k = 0), a dielectric (Si, n = 3.42, k = 0) and a metallic thin-film surface (n = 24.20, k = 24.66). Furthermore, we restrict the initial kinetic energies of the photoelectrons after excitation to three cases, 30 eV, 100 eV and 1 keV, that cover a wide range of commonly used energies in photoemission experiments. The incoming THz pulse (λ = 150 µm, FWHM = 5 ps) is linearly polarized either perpendicular (s) (Fig. 3) or parallel (p) (Fig. 4) to the plane of incidence with an incidence angle α = 60° with respect to the surface normal. The amplitude of the incoming THz pulse is $7 \cdot 10^7$ V/m in all simulations.

The Monte-Carlo simulations in absence of a transient grating, i.e. with no surface present (Fig. 3(a)), show that the incoming electric field is nicely reconstructed both in amplitude and shape over the wide range of kinetic energies between 30 eV and 1 keV. This is the proof-of-principle case for our reconstruction scheme. Simulations performed on the metallic (Fig. 3(b)) and dielectric surface (Fig. 3(c)) also result in Gaussian-shaped electric fields with identical temporal behavior at each kinetic energy. The amplitudes are smaller compared to the transparent case. Reconstructed peak amplitudes at the metallic substrate are estimated to be $1.7 \cdot 10^6$ V/m at 30 eV, $1.5 \cdot 10^6$ V/m at 100 eV and $3.2 \cdot 10^6$ V/m at 1 keV. At the Si interface the peak amplitudes are $1.8 \cdot 10^7$ V/m (30 eV), $1.7 \cdot 10^7$ V/m (100 eV) and $1.5 \cdot 10^7$ V/m (1 keV),

Optics EXPRESS

indicating that for both cases, metallic and dielectric, the peak amplitude depends on the initial kinetic energy of the electron.

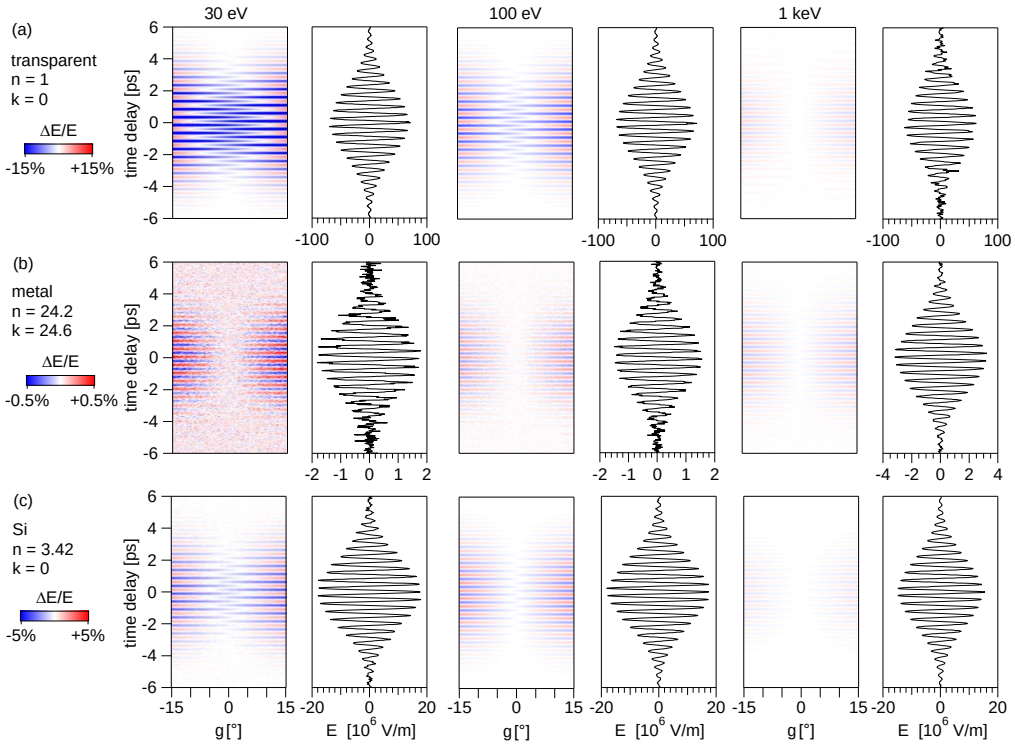

Fig. 3. Monte-Carlo simulations showing the relative change in electron kinetic energy as a function of detection angle due to the influence of the THz field. The respective reconstructed electric fields for a s-polarized ($E_{\parallel}$) Gaussian THz pulse with an amplitude of $7 \cdot 10^7$ V/m, an incidence angle α = 60°, and a pulse duration of FWHM = 5 ps are shown next to the COM maps. The simulations are performed on a transparent, a metallic and a dielectric sample surface at different initial photoelectron kinetic energies.

In Fig. 4 Monte-Carlo simulations are shown with the electric field polarized in the plane of incidence (p-pol). The field amplitude for the transparent case at 30 eV kinetic energy (Fig. 4(a)) is $6.1 \cdot 10^7$ V/m and hence around 13% smaller as compared to the input pulse. At the metallic and dielectric surface (Figs. 4(b) and 4(c)) an increase in amplitude to $1.2 \cdot 10^8$ V/m (metal, 30 eV) and $7.7 \cdot 10^7$ V/m (Si, 30 eV) is observed. In addition, a small dependency on the kinetic energy which leads to a decrease in peak amplitude with higher initial electron energy, e.g. a decrease from $6.1 \cdot 10^7$ V/m at 30 eV to $5.8 \cdot 10^7$ V/m at 1 keV at the transparent interface, can be observed. This trend is present on all interfaces investigated.

Optics EXPRESS

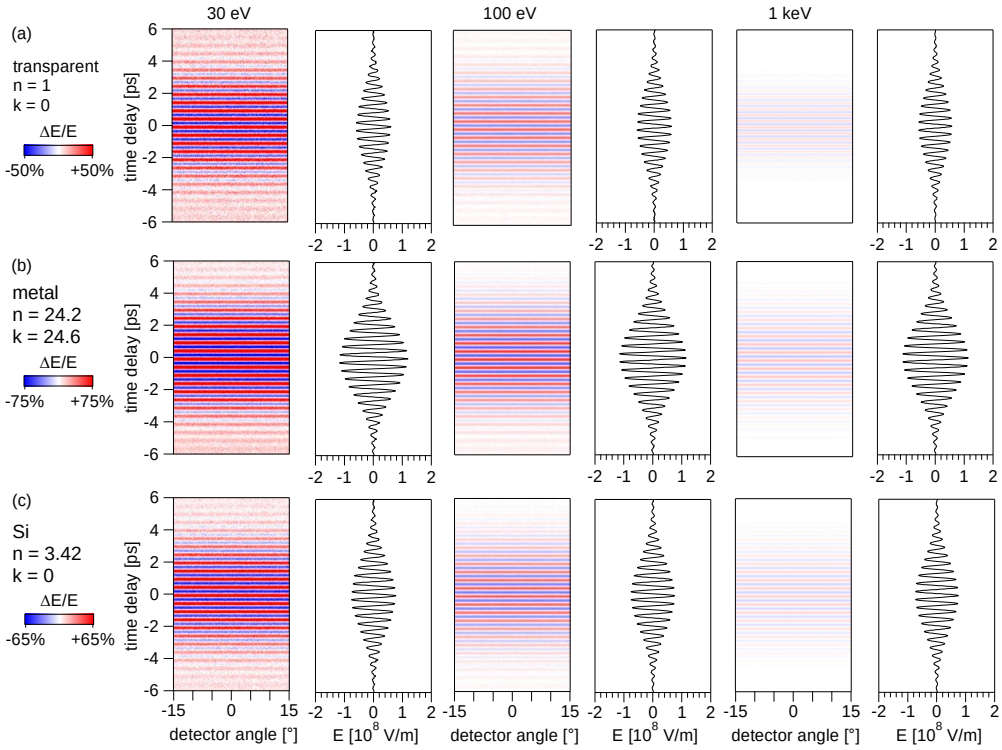

Fig. 4. Same as in Fig. 3, but for a p-polarized Gaussian THz pulse ($E_{\perp}$) with an amplitude of $7 \cdot 10^7$ V/m, incidence angle $\alpha = 60°$ and FWHM = 5 ps.

Figure 5(a) shows the ($E_{\parallel}$)-component as a function of initial electron energy for the interface-free case. The field strength of the incoming pulse is reconstructed within a residual 5% error for the cases of 30 eV and 100 eV. At 1 keV the relative error increases towards the shoulders of the Gaussian-pulse. The reconstructed electric field is smaller than the input field in all cases. In Fig. 5(b) the same information is presented for the case of the perpendicular polarized field component. At 30 eV and 100 eV kinetic energy, the residual error of the reconstruction scheme is below 5% for the main part of the pulse between ± 4 ps. The mostly negative values of the residuals again show a reduced field strength as compared to the input field. At 1 keV kinetic energy the field is slightly further underestimated (~-6%). In Fig. 5(c) we investigated the influence of a longer XUV probe pulse. The longer 100 fs probe pulse leads to a slightly larger residual error of around 8%.

Optics EXPRESS

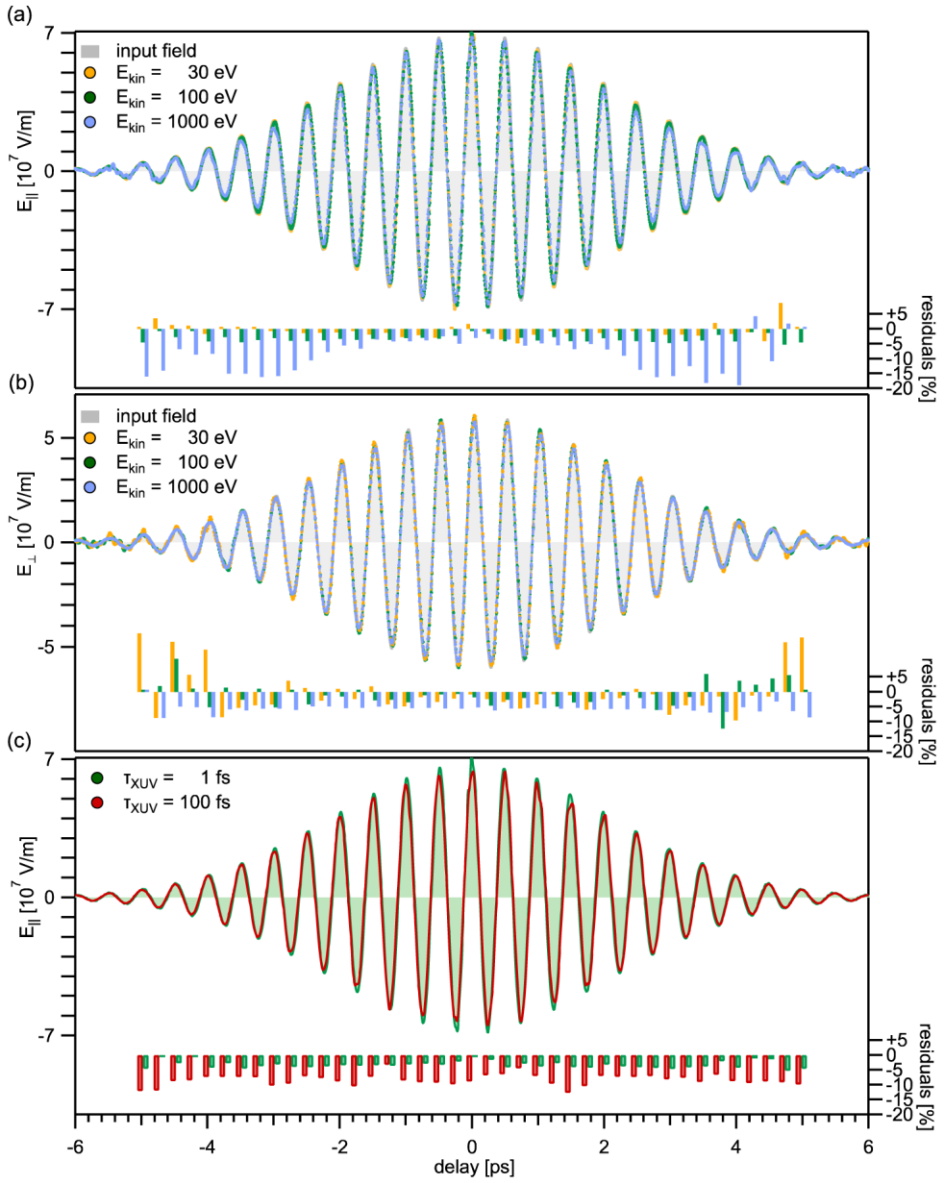

Fig. 5. Reconstructed fields as a function of time delay at the surface of a perfectly transparent material. (a) Reconstructed fields of a s-polarized Gaussian THz pulse ($E_{\parallel}$) with an amplitude of $7{\cdot}10^7$ V/m, an incidence angle of α = 60°, and a pulse duration of FWHM = 5 ps for different initial electron energies. (b) Same as (a) but for a p-polarized Gaussian THz pulse ($E_{\perp}$). (c) Reconstructed field of a s-polarized Gaussian THz pulse as in (a) for two different XUV pulse durations τ_{XUV}. The kinetic energy of the electrons is 100 eV in both cases. The residuals show the relative difference between the reconstructed and the input pulse.

4. Discussion

The case of a perfectly transparent interface in Fig. 5 shows that our reconstruction method is suitable to extract the field amplitude of the THz-pulse. Residual errors are around 5% of the input field strength. The reconstructed field is smaller due to the electron motion within the interaction time of electron and light pulse. As a consequence the field is not sampled at one specific point in space. An electron with 30 eV kinetic energy travels a distance of around 16

Optics EXPRESS

μm (normal emission) within a THz interaction interval of 5 ps. This is a non-negligible fraction of the wavelength (here 150 μm) and hence the electron enters regions of the field that show different amplitudes compared with the amplitude at the point of electron emission. The higher the electron velocity, the more significant this effect.

In case the THz pulse hits a partially reflective interface (Figs. 3(b) and 3(c)) a 2D transient field grating builds up. The reconstructed field components in parallel polarized cases have smaller amplitudes due to destructive interference of the incoming and the reflected waves close to the surface. The reconstructed field strength at the metallic interface is $1.5 \cdot 10^6$ V/m (100 eV) and hence only 2% of the incoming peak amplitude. For the silicon interface the reconstructed peak amplitude is $1.8 \cdot 10^7$ V/m at 100 eV. Here, Fresnel's equations result in a reflectivity of R = 54% at 60° incidence angle. The phase of the complex coefficient of reflection is $-\pi$ in this case leading to a peak amplitude of

$$\left|E_{\parallel,\max}\right| = \sqrt{\left|E_{\parallel,i}\right|^2 + \left|E_{\parallel,r}\right|^2 + 2 \cdot \left|E_{\parallel,i}\right|\left|E_{\parallel,r}\right| \cos(\phi_\parallel)} = 1.84 \cdot 10^7 \frac{\mathrm{V}}{\mathrm{m}} \qquad (4)$$

$\left|E_{\parallel,i}\right|$ and $\left|E_{\parallel,r}\right|$ are the electric field moduli of the incoming and reflected pulse corresponding to the respective peak amplitudes. $\phi_\parallel$ is the phase shift of the reflected wave. The result is in reasonable agreement with our reconstructed amplitude (Fig. 4(c)). The dependency on the initial kinetic energy of the electrons is again due to the electron motion during the field interaction time. At higher energies, the electrons have travelled a longer distance within the 2D field distribution in a certain time interval and hence their momentum gain is a result of the acting field at different locations along their path. This in turn differs from the instantaneous field at a specific position in space, for example the substrate surface.

In case of the THz pulse polarized perpendicular to the surface, we determine an electric field amplitude at the transparent substrate that is 14% smaller than the total input field strength due to the oblique angle of incidence of 60°. Electric field amplitudes for the reflected fields at metallic and dielectric interfaces are larger compared to the situation without reflection due to constructive interference (Figs. 4(b) and 4(c)). At the metallic interface where the reflectivity is around 84% the initial field strength is almost doubled ($1.2 \cdot 10^8$ V/m, 30 eV). In case of Si with a reflectivity of around 7.6% at 60° incidence angle the total amplitude perpendicular to the substrates surface is then $7.7 \cdot 10^7$ V/m following Eq. (4). We indeed observe an amplitude enhancement in the reconstruction of around 10% (Fig. 4(c)). At all interfaces a tendency of decreasing peak amplitudes with increasing electron energy can be understood by taking the electron motion in the field grating into account (Fig. 5(b)).

We have shown that our pulse reconstruction scheme is suitable to determine the strength of both field components parallel and perpendicular to different substrate surfaces. Thus, arbitrarily polarized fields can be reconstructed. In case of circularly or elliptically polarized light the amplitude of the individual components varies with the frequency of the incoming field. Here, $E_\parallel$ and $E_\perp$ can be reconstructed at any instant using our method, and the phase shift can be determined from the temporal profiles of both components. The dependence of the reconstructed field amplitude on the initial kinetic energy of the electrons sets a limit to the accuracy of the reconstruction since the field grating is not sampled at a specific location. As a guideline it can be said, that the initial electron energy has to be selected so that the distance Δs travelled by the electron at a speed v_e during the interaction with the THz field is significantly shorter than the wavelength of the investigated field projected along the direction of electron detection:

$$\frac{\Delta s}{\lambda \cdot \cos(\alpha)} = \frac{v_e \cdot \tau_{THz}}{c \cdot \cos(\alpha) \cdot T_{THz}} = \frac{v_e}{c \cdot \cos(\alpha)} \cdot n \ll 1 \Leftrightarrow E_{kin} \ll \frac{m \cdot c^2}{2n^2} \cdot \cos^2(\alpha). \qquad (5)$$

Optics EXPRESS

Here, the THz pulse duration is τ_{THz} and the period of the field is T_{THz} which result in n optical cycles of the light pulse. c is the speed of light and α the angle of light incidence as defined in Fig. 1(a). In our simulated cases where we use a 10 cycle pulse at 60° incidence the kinetic energy should be smaller than 640 eV. Furthermore, the spatial and temporal dimension of the probing XUV pulse has to be small compared to the dimensions of the THz-pulse in order to meet the sampling conditions in space and time. In particular the reconstruction of the peak amplitude of few-cycle pulses requires significant oversampling compared to the Nyquist rate. An additional timing jitter between XUV and THz pulses typical for FEL experiments can be incorporated into a Gaussian broadening of the XUV probe pulse. In Fig. 5(c) we show a reconstruction using a longer 100 fs XUV probe pulse. Even in this scenario, the error of the reconstructed peak amplitude is below 8%. Finally, it should be noted that the reconstructed amplitude corresponds to the spatially-averaged THz field in the XUV probe volume.

5. Summary

We developed a polarization-resolved near-surface electric field reconstruction method based on the energy- and angular-resolved detection of electron distributions modified by an acting electromagnetic field. The method is sensitive for the detection of electric field amplitudes at interfaces with a broad variety of optical properties. The ease of integration into existing photoelectron spectroscopy setups makes this approach available to a wide variety of pump-probe experiments.

Appendix

Equation (1) can be derived using vector algebra. For a linear polarization the final state momentum $\mathbf{p'}$ is given by

$$|\mathbf{p'}|^2 = \langle \mathbf{p'}|\mathbf{p'}\rangle = \langle \mathbf{p}+\Delta\mathbf{p}|\mathbf{p}+\Delta\mathbf{p}\rangle = |\mathbf{p}|^2 + |\Delta\mathbf{p}|^2 + 2|\mathbf{p}||\Delta\mathbf{p}|\langle\hat{\mathbf{p}}|\Delta\hat{\mathbf{p}}\rangle. \quad (6)$$

Here, $\mathbf{p}$ is the initial electron momentum vector related to the electron kinetic energy without any dressing laser field. $\Delta\mathbf{p}$ corresponds to the added electron momentum due to interaction with the field. $\Delta\hat{\mathbf{p}}$ and $\hat{\mathbf{p}}$ are unit vectors in the respective directions. Assuming a parabolic, non-relativistic free-electron dispersion and identifying the scalar product in the last term as (see Fig. 1)

$$\langle\hat{\mathbf{p}}|\Delta\hat{\mathbf{p}}\rangle = \cos(\gamma) \quad (7)$$

for pure perpendicular polarization. The final state electron energy is

$$E' = E + \frac{1}{2m}|\Delta\mathbf{p}_\perp|^2 + \frac{1}{m}|\mathbf{p}||\Delta\mathbf{p}_\perp|\cos(\gamma). \quad (8)$$

In case of pure perpendicular polarization the kinetic energy offset between final and initial electron energy at small observation angle $\gamma \approx 0^\circ$ is

$$\Delta E'|_{\gamma\sim 0^\circ} = \pm\frac{1}{m}|\mathbf{p}||\Delta\mathbf{p}_\perp|. \quad (9)$$

Here, we assume that $|\Delta\mathbf{p}_\perp|$ is small compared to $|\mathbf{p}|$, i.e. the energy offset gained due to the field interaction is small compared to the electrons initial kinetic energy E obtained in the photoemission process. If the energy offset is not small compared to the electrons initial kinetic energy the absolute momentum gain can be obtained solving the quadratic equation [Eq. (7)].

Optics EXPRESS

$$|\Delta\mathbf{p}| = |\mathbf{p}|\left(\sqrt{1+\frac{2m\Delta E}{|\mathbf{p}|^2}}-1\right) = \sqrt{2mE}\left(\sqrt{1+\frac{\Delta E}{E}}-1\right) \tag{10}$$

A polarization direction parallel to the surface leads to modifications in the absolute value and direction of the electron momentum. Here, the initial emission direction is unknown which precludes an analytical relation between the experimental parameter tilt angle and the absolute momentum gained. The tilt angle of the COM energy distribution in Fig. 1(c) is nevertheless a hallmark of the momentary direction of the parallel field component. By taking the temporal shape of the tilt angle as the temporal shape of the vector potential, it can be used as input to our model. We simulate the tilt angle at every point during the laser interaction time as a function of the electric field amplitude by adjusting the amplitude to minimize the deviation between simulated and real tilt angle at all times in a least square fit fashion.

In addition to the perpendicular field component, p-polarized light can have a component parallel to the surface. This component will influence the energy offset detected along normal emission. Qualitatively, the contribution to the overall offset will be a reduction in energy that varies in time with twice the frequency of the THz field. However, if the initial electron momentum is much larger than the parallel momentum gained due to the field interaction, the influence of this component is negligible:

$$\left|\Delta\mathbf{p}_\perp\right|_{\|,\gamma'\to 0^\circ} = \left|\Delta\mathbf{p}_\|\right| \cdot \tan(\gamma'). \tag{11}$$

Here, $\left|\Delta\mathbf{p}_\perp\right|_{\|,\gamma'\to 0^\circ}$ is the momentum change detected perpendicular to the surface due to the parallel field component. $\left|\Delta\mathbf{p}_\|\right|$ is the total added momentum in direction parallel to the surface by the p-polarized pulse and γ' is the polar emission angle of electrons in a field free situation that are pushed to normal direction due to the THz interaction. A comparison of $\left|\Delta\mathbf{p}_\perp\right|_{\|,\gamma'\to 0^\circ}$ with $\left|\Delta\mathbf{p}_\perp\right|$, the added momentum due to the perpendicular component, results in

$$\frac{\left|\Delta\mathbf{p}_\perp\right|_{\|,\gamma'\to 0^\circ}}{\left|\Delta\mathbf{p}_\perp\right|} = \frac{\left|\Delta\mathbf{p}_\|\right|}{\left|\Delta\mathbf{p}_\perp\right|} \cdot \tan(\gamma') \sim \frac{\sin(90^\circ-\alpha)}{\cos(90^\circ-\alpha)} \cdot \tan(\gamma'), \tag{12}$$

where α is the incidence angle of the light. The assumption that the added momentum in direction parallel to the surface is much smaller than the initial photoelectron momentum leads to $\gamma' \to 0^\circ$ and hence a negligible contribution of the parallel component on the reconstructed perpendicular field.

Funding

NCCR Molecular Ultrafast Science and Technology (NCCR MUST); Swiss National Science Foundation (SNSF).